

Cave Volume Estimation in Python

Timm Hopp

Analysis and Modeling
Summer Term 2025

Abstract

Scientific literature regarding caves overlooked the calculation of volumes for most parts. While current software is able to plot caves in 3D, no accessible methods of volume calculation seem to exist at the moment. In this project, I aimed to close this gap. By using cave survey data and treating cave segments as elliptical truncated cones in 3D space, the overall volume could be calculated. To avoid error stemming from segments originating in the same point and thus overlapping, these intersecting volumes were identified and calculated. The method was shown to fulfill the task and be geometrically and mathematically sound.

June 6, 2025

1 Introduction

Interest in caves can be found in travel reports for centuries, but only at around the turn of the 19th to the 20th century, speleology was started as an independent scientific discipline to map and research cave systems in an academic way. With the founding of speleological societies and advancements in the engineering of measuring devices, detailed maps could be first created to reveal and display the data. Scientific disciplines from geology and biology to social and historical studies showed and continued to show great interest into these new discoveries.

In modern times, a great number of surveys have been undertaken and caves mapped throughout the world. Still today, measurements are mostly made using traditional equipment where distances are taken through tape measures or inclination and orientation using geological compasses and clinometers. (Mattes, 2015) While newer devices and technologies like laser scanners (Gallay et al., 2016) or photogrammetry (Cazes et al., 2024) allow for accurate measurements, their use remains impractical. Laser scanning equipment is expensive and can be unwieldy when carried through caves. Especially when caves contain narrow passages or areas with water, the equipment is at risk of being damaged or not usable. Cazes et al., 2024 showed that photogrammetry can help here, as the results can be comparable to those of LiDAR scans, however lighting remains an issue. At the same time cameras are at the same risk of water or physical damage. As a result of these limitations, classical methods remain important. However, these measurements are lacking in details as measurements are taken at specific points only and cannot reproduce the complexity of a cave. Rather, they can only give a general idea of a cave's physical structure. Mattes, 2015 additionally notes the importance of "verbal descriptions and photos" to give an understanding to people who have not been to the cave. Nevertheless, these measurements, while not being able to completely reproduce the surveyed areas, can help give an understanding of their geological and hydrological histories and act as a basis for different fields of research. Countless studies on different caves around the world exist and were used for further scientific inquiry.

In the field of speleology and cave surveying, the focus remains on a cave's structure, length, and extensions or dimensions. However, an area that has gained little research is cave volumes. While some studies exist in which researchers tried to calculate individual volumes, no universal framework for calculations can be identified. Volume calculations on irregularly shaped objects have been shown to function based on 3D point clouds from laser scans or photogrammetry by Wang et al., 2023 or Lee et al., 2012 but literature on cave specific volumes remains extremely limited. Jakopin, 1981 introduced a method for estimating volumes based on reducing segments of a cave to truncated cones. Digital implementations of this method do not seem to exist. While some basic volume calculation is possible in the "Compass" software, Larson et al., 2013 showed that these are highly inaccurate. They proposed an alternative which, however, can not be found in detail online.

The goal of this project is to implement a Python pipeline, that takes cave survey data in traditional format as a table and calculates the volume of any given cave. Volumetric inquiry remains widely overseen but could eventually help gather new understandings of caves, geological and hydrological processes and pasts. To test the proposed software, it will be applied on theoretical possible cave shapes and intersections and eventually survey data of a cave system in the Untersberg mountain in Germany and Austria. As the topic of cave volume allows for no practical methods for verifying calculated results, the project will utilize geometric calculations to achieve a mathematically sound result.

2 Methods

To implement the volume estimation, a pipeline will be created in a Python program. After an initial data-formatting, different volumes of the cave system will be calculated and combined under consideration of topology. The total volume will need adjustment as sections might overlap or show missing values in transition areas between segments.

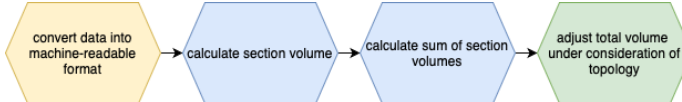


Figure 1: Workflow of the suggested pipeline

2.1 Data

Data for practical implementation of this project was collected in different cave systems inside the Untersberg mountain on the Austrian-German border. It consists of multiple tables for each cave. These are divided into segments with information about length, inclination, and bearing. At each measuring point distances to the bottom, top, left, and right are provided. The data currently exists in a collection of spreadsheets with multiple tables of measurements taken by hand. Figure 2 shows such measurements.

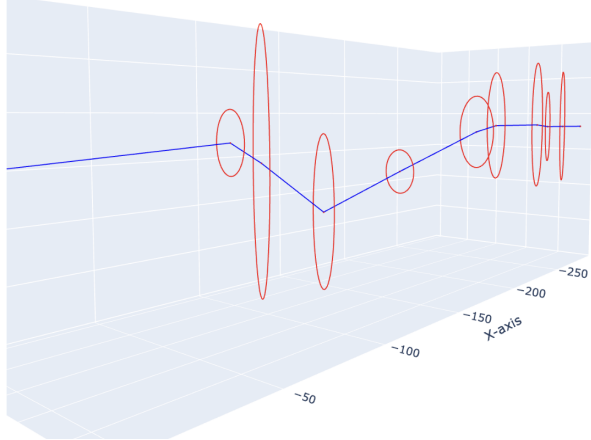


Figure 2: Ellipses drawn from measurements

2.2 Data preprocessing

As the data is currently in a format that is not readily readable by a machine, initial formatting will be necessary. The tables currently provided will be gathered in a single file as comma-separated values (CSV) and an additional column added to indicate the cave or section of a cave, allowing processing these individually and calculating their specific volumes. No additional data preprocessing for initial segment volume calculations will be necessary, as the data was collected at points at different distances, making the data able to be treated as given in sections. The table will be read and subsequently processed using the Pandas library (McKinney et al., 2010) for Python. The resulting table can be found in Appendix A.

2.3 Section volume calculation

Given the format in which data was provided, the cave segments can be geometrically reduced and handled as (elliptic) cylindrical structures or truncated cones. In case measurements of two subsequent measurement points being the same, the volume formula for an elliptic cylinder could be applied.

$$V = \pi * l * h * w$$

where:

- l = length of the section
- h = height of the section
- w = width of the section

As this is unlikely and measurements will in most, if not all, cases differ

between the points, volume will be calculated for a truncated cone.

$$V = \frac{1}{3}\pi * l * (w_1 h_1 + w_2 h_2 + \sqrt{w_1 h_1 \cdot w_2 h_2})$$

where:

w_1, h_1 = semi-axis in width, height at first measuring point

w_2, h_2 = semi-axis in width, height at second measuring point

l = length of the section

The values will be calculated from the distances provided in the data with height being the sum of the "UP" and "DOWN" values and width "LEFT" and "RIGHT", respectively. The length is provided as "LENGTH". Calculations will be done segment by segment using the Numpy library (Harris et al., 2020). Focusing on one formula only eliminates operations for comparing beginning and end measurements and reduce computation time and resources needed.

2.4 Final volume adjustment

As the system's caves are provided and calculated as segments, adjustments to total calculated volume will have to be made. While the sum of all segments can provide a good estimation, intersections between segments can lead to inaccuracies as overlapping areas would be added twice to the volume. Figure 3 shows such a case.

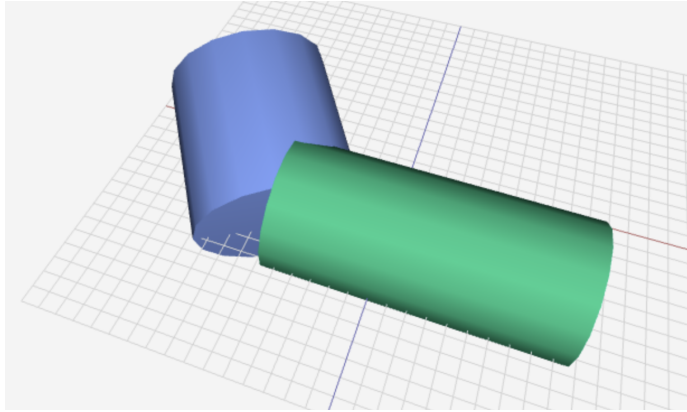


Figure 3: Intersection of two cave segments

Using the inclination and orientation of the measurements, the segments can be projected into 3D space and their intersection calculated. However, the computations for finding and calculating these intersections are complex and complicated. Especially numerical calculations of intersections of objects in three-dimensional space are computationally expensive and, while highly accurate, do not seem necessary under consideration of limitations stemming from

the measurement process mentioned before. As an alternative, voxelization will therefore be used. The segments will be transformed into voxels and compared, with those present in multiple segments representing intersection volumes. Although some accuracy is lost in the voxelization process, these inaccuracies can be reduced by higher resolutions. Furthermore, the resulting error can be ignored given the inaccuracies from surveying mentioned above.

In a first step, cave segments are considered as their outer surfaces in R^3 . These can be formalized as:

$$\begin{aligned}\vec{X}(u, v) = & \vec{P}_0 + u \vec{d} + [(1 - u) * r_{1a} + u * r_{2a}] + \cos(v) * \vec{e}_1 \\ & + [(1 - u) * r_{1b} + u * r_{2b}] + \sin(v) * \vec{e}_2\end{aligned}\quad (1)$$

where:

- \vec{P}_0 = the center of the start ellipse
- \vec{P}_1 = the center of the end ellipse
- $u \in [0, 1]$ = the interpolating parameter of the height of the cone from \vec{P}_0 to \vec{P}_1
- $v \in [0, 2\pi]$ = the angle parameter describing the ellipses
- \vec{d} = the vector along the centreline $\vec{P}_1 - \vec{P}_0$
- e_1, e_2 = the orthonormal vectors to \vec{d}

By using orientation and inclination from the survey as rotations around the x- and y-axis respectively, the segments can be topologically corrected and put in their relationship. Orientation is calculated by multiplying the segment by the rotation matrices

$$R_x = \begin{bmatrix} 1 & 0 & 0 \\ 0 & \cos(\alpha) & -\sin(\alpha) \\ 0 & \sin(\alpha) & \cos(\alpha) \end{bmatrix}$$

and

$$R_y = \begin{bmatrix} \cos(\beta) & 0 & \sin(\beta) \\ 0 & 1 & 0 \\ -\sin(\beta) & 0 & \cos(\beta) \end{bmatrix}$$

where:

- α = rotation around x (polar orientation)
- β = rotation around y (inclination)

The resulting reoriented segments will then be voxelized, as shown in Figure 4, and intersecting voxels counted, resulting in the intersecting volume to be extracted from the total volume of all segments.

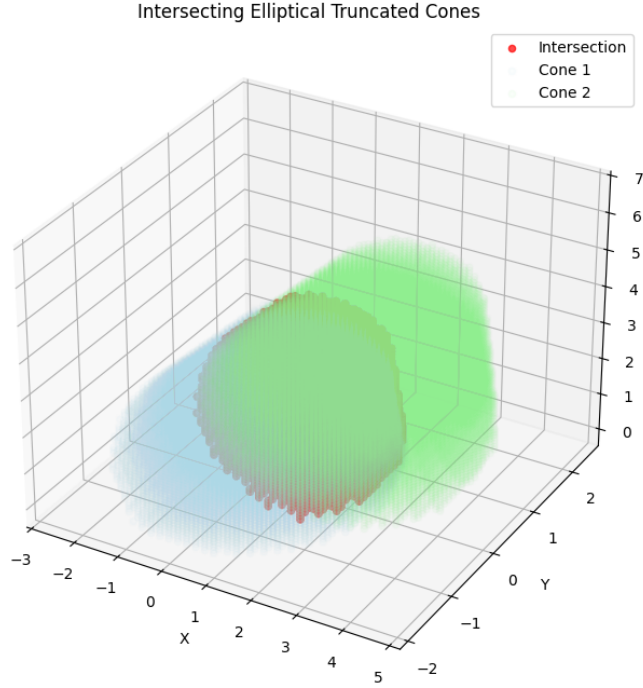


Figure 4: Voxalized intersection of two segments

As the calculation returns a number of voxels without specified volume, it is important to choose the axis limits and resolution according to the data. The volume of a single voxel can then be calculated by as:

$$V_{voxel} = \frac{\|x_{max} - x_{min}\|}{resolution} * \frac{\|y_{max} - y_{min}\|}{resolution} * \frac{\|z_{max} - z_{min}\|}{resolution}$$

for the minimum and maximum values of each axis. Figure 5 shows a possible grid at a resolution of 25, dividing every axis into 25 equally sized chunks with a voxel volume of 0.256m^3 .

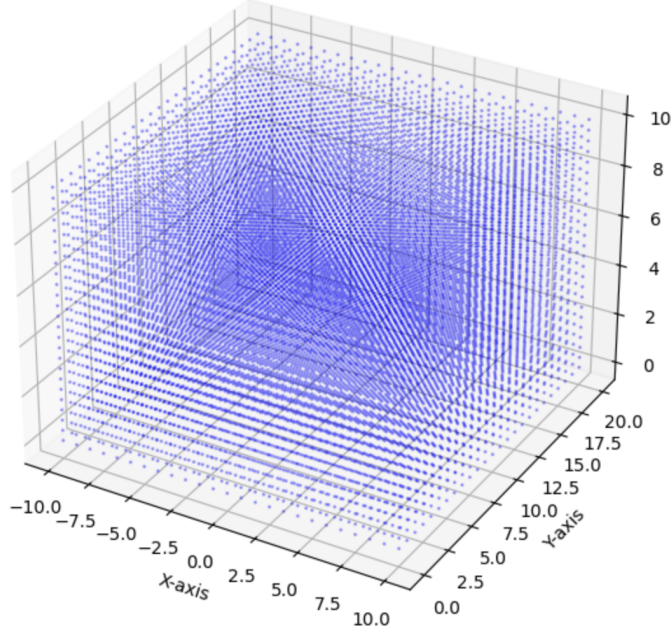


Figure 5: Center points of voxel grid

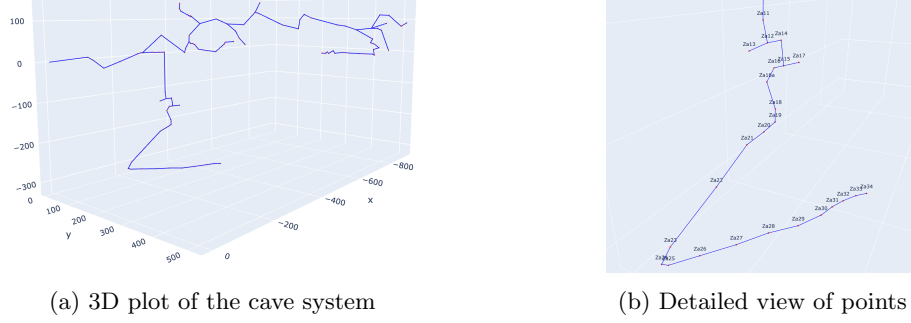
3 Experiments

The proposed method was tested on surveyed data from a cave system containing multiple connected caves, spanning a total of 3271.81m in length and 114 measurement points. The full table of measurements can be found in Appendix A.

To process the data, measurement points were projected into 3D. The first measurement was taken to be at $\begin{bmatrix} 0 \\ 0 \\ 0 \end{bmatrix}$ and subsequent points calculated as

$$\begin{aligned} dx &= \text{LENGTH} \cdot \cos(\text{CLINO}) * \sin(90-\text{COMPASS}) \\ dy &= \text{LENGTH} \cdot \cos(\text{CLINO}) * \cos(90-\text{COMPASS}) \\ dz &= \text{LENGTH} \cdot \sin(\text{CLINO}) \end{aligned}$$

Figure 6 shows the entire cave system used in the calculations, as well as a detailed view of the according survey points projected into R^3 .



(a) 3D plot of the cave system

(b) Detailed view of points

Figure 6: Cave system plotted from measurement points and center line

The projected points were saved into a dictionary to be later accessed for calculating intersection volumes as explained above.

3.1 Sectional Calculation

Using the above mentioned formula for volumes of elliptical truncated cones, the data was parsed row by row and each sections volume was calculated. The volume of the surveyed cave system was calculated to be around 782375.17m³. A detailed list of all segment volumes can be found in Appendix B.

3.2 Intersection Correction

To check for possibly overlapping segments, points from which multiple caves originated were taken and checked against each other for possible intersecting volumes. However, no such cases were found in the data.

To test the proposed method, measurements of a cave consisting of 4 segments were artificially created. By choosing cylindrical segments in one plane, the intersecting volume had the shape of a Steinmetz solid, the volume of which can be calculated as $V = \frac{16}{3}r^3$.

Table 1: Intersecting segments measurements

from	to	length	compass	clino	left	up	down	right
T1	T2	10	90	0	-2	2	-2	2
T2	T3	10	90	0	-2	2	-2	2
T2	T4	10	0	0	-2	2	-2	2
T2	T5	10	180	0	-2	2	-2	2
T2	T6	10	270	0	-2	2	-2	2

Table 1 shows the measurements used. A radius of 2 was chosen via the distances at the survey points. The right angles in the compass measurements

allowed for considering two opposing segments to be considered as a single cylinder for comparison to the Steinmetz solid volume. Figure 7 shows the according center lines.

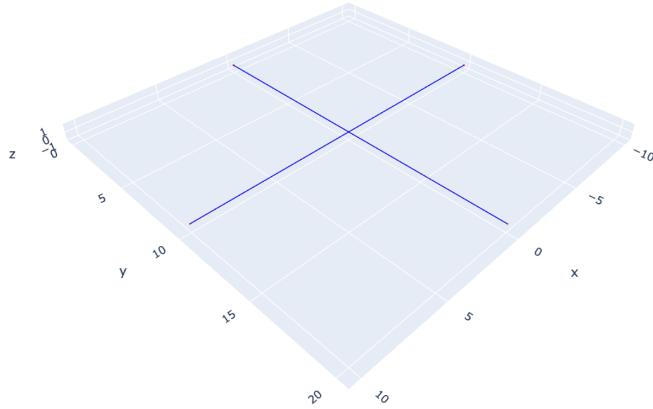


Figure 7: Intersecting cylindrical segments

The sectional volumes were calculated as 125.66m^3 each, totaling to 502.64m^3 for the entire cave without corrections. An intersecting volume of 45.57m^3 was calculated at a resolution of 400. This is roughly in line with the reference result of 42.67m^3 . The discrepancy can be explained through the measurement using voxels. As only full voxels within the volumes are measured, accuracy is lost closer to the outer surface of the cylinders. Table 2 shows the results for different resolutions.

Table 2: Intersecting Volume at Different Resolutions

Resolution	Intersecting Volume in m^3
10	74.07
25	43.94
50	48.48
100	45.14
200	45.72
250	46.18
300	46.17
350	46.16
400	45.57

4 Discussion

The proposed method was shown to be useful in approximating cave volumes. By projecting the measurement points into a three-dimensional coordinate system and treating segments as elliptical truncated cones, the overall volume could be calculated. While some discrepancy remains in calculating intersecting volumes, the approach reached an acceptable result while keeping processing time and required computational resources low. A higher resolution during voxalization might have led to more accurate results; however, very high RAM usage required for such calculations was not feasible. Additionally, as the measurements and representations of cave segments as cones are already highly abstracted, the error could possibly be ignored. Although the calculations are mathematically sound, there is no way of experimentally proving the results. The data used limits the application on older surveys in similar format. Modifying the code to calculate volumes of more complex shapes derived from more accurate measurements could help calculating volumes from newer surveys in the future.

The code will be made accessible at <https://github.com/timmhopp/CaveVolume>

References

- Mattes, J. (2015). Underground fieldwork—A cultural and social history of cave cartography and surveying instruments in the 19th and at the beginning of the 20th century. *International Journal of Speleology*, 44(3), 251–266. <https://doi.org/10.5038/1827-806X.44.3.4>
- Gallay, M., Hochmuth, Z., Kaňuk, J., & Hofierka, J. (2016). Geomorphometric analysis of cave ceiling channels mapped with 3-D terrestrial laser scanning. *Hydrology and Earth System Sciences*, 20(5), 1827–1849. <https://doi.org/10.5194/hess-20-1827-2016>
- Cazes, G., Vernant, P., Baleux, F., Giuliani, C., Brugal, J.-P., & Jouves, J. (2024). Full size cave 3d modelling using close range photogrammetry and comparison with laser scanning. <https://doi.org/10.21203/rs.3.rs-4849312/v1>
- Wang, Y., Ding, M., Zhang, Q., Zhang, X., & Qu, Z. (2023). Volume calculation methods of irregular stone artifacts based on 3D laser scanning technology. *Journal of Asian Architecture and Building Engineering*, 22(6), 3386–3402. <https://doi.org/10.1080/13467581.2023.2182640>
- Lee, Y., Cho, S.-Y., Kim, K., & Lee, D.-G. (2012). The Stereo Camera Measurement of Point Cloud on 3D Object and the Calculation of Volume Based on Irregular Triangular Mesh. *The Journal of The Institute of Internet, Broadcasting and Communication*, 12(4), 153–159. <https://doi.org/10.7236/JIWIT.2012.12.4.153>
- Jakopin, P. (1981). On Measuring Caves by Volume. *Proceedings of the 8th international congress of speleology, Bowling Green 1981*, 270–272. http://www.jakopin.net/primoz/clanki/1981_MCV/index.php
- Larson, E. B., Travis, R. W., & Mylroie, J. E. (2013). Cave Volume Calculations and Corrections Using the Compass Software. https://gsa.confex.com/gsa/2013AM/webprogram/Paper225016.html?utm_source=chatgpt.com
- McKinney, W., et al. Data structures for statistical computing in python. In: In *Proceedings of the 9th python in science conference*. 445. Austin, TX. 2010, 51–56.
- Harris, C. R., Millman, K. J., van der Walt, S. J., Gommers, R., Virtanen, P., Cournapeau, D., Wieser, E., Taylor, J., Berg, S., Smith, N. J., Kern, R., Picus, M., Hoyer, S., van Kerkwijk, M. H., Brett, M., Haldane, A., del Río, J. F., Wiebe, M., Peterson, P., ... Oliphant, T. E. (2020). Array programming with NumPy. *Nature*, 585(7825), 357–362. <https://doi.org/10.1038/s41586-020-2649-2>

A Cave Measurements

FROM	TO	LENGTH	COMPASS	CLINO	LEFT	RIGHT	UP	DOWN
Ja5	Za1	94.82	161.00	94.82	94.82	94.82	94.82	94.82
Za1	Za2	18.04	177.00	18.04	18.04	18.04	18.04	18.04
Za2	Za3	33.14	141.00	33.14	33.14	33.14	33.14	33.14
Za3	Za4	51.18	175.00	51.18	51.18	51.18	51.18	51.18
Za4	Za5	52.17	163.00	52.17	52.17	52.17	52.17	52.17
Za5	Za6	10.50	103.00	10.50	10.50	10.50	10.50	10.50
Za6	Za7	36.42	171.00	36.42	36.42	36.42	36.42	36.42
Za7	Za8	6.56	147.00	6.56	6.56	6.56	6.56	6.56
Za8	Za9	12.47	165.00	12.47	12.47	12.47	12.47	12.47
Za9	Za10	11.48	146.00	11.48	11.48	11.48	11.48	11.48
Za10	Za11	5.58	186.00	5.58	5.58	5.58	5.58	5.58
Za11	Za12	110.24	0.00	110.24	110.24	110.24	110.24	110.24
Za12	Za13	18.37	80.00	18.37	18.37	18.37	18.37	18.37
Za13	Za14	17.39	321.00	17.39	17.39	17.39	17.39	17.39
Za13	Za15	16.08	160.00	16.08	16.08	16.08	16.08	16.08
Za15	Art	40	-170.00	40	40	40	40	40
Za15	Za16	22.31	140.00	22.31	22.31	22.31	22.31	22.31
Za16	Za17	9.84	327.00	9.84	9.84	9.84	9.84	9.84
Za16	Za16a	20.67	162.00	20.67	20.67	20.67	20.67	20.67
Za17	Za18	13.78	330.00	13.78	13.78	13.78	13.78	13.78
Za18	Za19	31.17	168.00	31.17	31.17	31.17	31.17	31.17
Za19	Za20	12.80	0.00	12.80	12.80	12.80	12.80	12.80
Za20	Za21	14.76	333.00	14.76	14.76	14.76	14.76	14.76
Za21	Za22	20.01	326.00	20.01	20.01	20.01	20.01	20.01
Za22	Za23	47.57	336.00	47.57	47.57	47.57	47.57	47.57
Za23	Za24	67.26	329.00	67.26	67.26	67.26	67.26	67.26
Za24	Za25	20.01	314.00	20.01	20.01	20.01	20.01	20.01
Za25	Za26	6.17	125.00	6.17	6.17	6.17	6.17	6.17
Za26	Za27	30.51	148.00	30.51	30.51	30.51	30.51	30.51
Za27	Za28	39.04	149.00	39.04	39.04	39.04	39.04	39.04
Za28	Za29	39.37	151.00	39.37	39.37	39.37	39.37	39.37
Za29	Za30	37.07	144.00	37.07	37.07	37.07	37.07	37.07
Za30	Za31	34.12	152.00	34.12	34.12	34.12	34.12	34.12
Za31	Za32	25.10	167.00	25.10	25.10	25.10	25.10	25.10
Za32	Za33	20.34	157.00	20.34	20.34	20.34	20.34	20.34
Za33	Za34	20.83	147.00	20.83	20.83	20.83	20.83	20.83
Za34	Za35	17.06	143.00	17.06	17.06	17.06	17.06	17.06
Za6	HZ1	7.87	189.00	7.87	7.87	7.87	7.87	7.87
HZ1	HZ2	72.51	164.00	72.51	72.51	72.51	72.51	72.51
HZ2	HZ3	84.32	159.00	84.32	84.32	84.32	84.32	84.32
HZ3	HZ4	12.47	160.00	12.47	12.47	12.47	12.47	12.47
HZ4	HZ5	21.65	179.00	21.65	21.65	21.65	21.65	21.65

HZ5	HZ6	6.56	124.00	6.56	6.56	6.56	6.56	6.56
HZ6	HZ7	6.23	153.00	6.23	6.23	6.23	6.23	6.23
HZ7	HZ8	7.55	158.00	7.55	7.55	7.55	7.55	7.55
HZ8	HZ9	15.75	150.00	15.75	15.75	15.75	15.75	15.75
HZ9	HZ10	27.89	160.00	27.89	27.89	27.89	27.89	27.89
HZ10	HZ11	25.26	144.00	25.26	25.26	25.26	25.26	25.26
HZ11	HZ12	32.81	138.00	32.81	32.81	32.81	32.81	32.81
HZ12	HZ13	7.55	188.00	7.55	7.55	7.55	7.55	7.55
HZ13	HZ14	23.95	138.00	23.95	23.95	23.95	23.95	23.95
Za6	HZ1	7.87	189.00	7.87	7.87	7.87	7.87	7.87
HZ1	HZ2	72.51	164.00	72.51	72.51	72.51	72.51	72.51
HZ2	HZ3	84.32	159.00	84.32	84.32	84.32	84.32	84.32
HZ3	HZ4	12.47	160.00	12.47	12.47	12.47	12.47	12.47
HZ4	HZ5	21.65	179.00	21.65	21.65	21.65	21.65	21.65
HZ5	VH1	18.04	182.00	18.04	18.04	18.04	18.04	18.04
VH1	VH2	48.23	166.00	48.23	48.23	48.23	48.23	48.23
VH2	VHs1	45.93	265.00	45.93	45.93	45.93	45.93	45.93
VHs1	VHs2	19.36	222.00	19.36	19.36	19.36	19.36	19.36
VHs2	VHs3	25.59	238.00	25.59	25.59	25.59	25.59	25.59
VHs3	VHs4	25.92	311.00	25.92	25.92	25.92	25.92	25.92
VHs4	VHs5	10.17	305.00	10.17	10.17	10.17	10.17	10.17
VHs5	VHs6	17.39	54.00	17.39	17.39	17.39	17.39	17.39
VH2	VH3	47.90	131.00	47.90	47.90	47.90	47.90	47.90
VH3	VH4	38.71	161.00	38.71	38.71	38.71	38.71	38.71
VH4	VH5	31.50	136.00	31.50	31.50	31.50	31.50	31.50
VH5	VH6	24.28	103.00	24.28	24.28	24.28	24.28	24.28
VH6	VH7	24.61	144.00	24.61	24.61	24.61	24.61	24.61
HZ5	HZ6	6.56	124.00	6.56	6.56	6.56	6.56	6.56
HZ6	HZ7	6.23	153.00	6.23	6.23	6.23	6.23	6.23
HZ7	HZ8	7.55	158.00	7.55	7.55	7.55	7.55	7.55
HZ8	HZ9	15.75	150.00	15.75	15.75	15.75	15.75	15.75
HZ9	HZ10	27.89	160.00	27.89	27.89	27.89	27.89	27.89
HZ10	HZ11	25.26	144.00	25.26	25.26	25.26	25.26	25.26
HZ11	HZ12	32.81	138.00	32.81	32.81	32.81	32.81	32.81
HZ12	HZ13	7.55	188.00	7.55	7.55	7.55	7.55	7.55
HZ13	HZ14	23.95	138.00	23.95	23.95	23.95	23.95	23.95
VH4	VH8	51.61	151.50	51.61	51.61	51.61	51.61	51.61
VH8	VH9	53.90	164.20	53.90	53.90	53.90	53.90	53.90
VH9	VH9a	34.58	175.50	34.58	34.58	34.58	34.58	34.58
VH9	VH10	9.12	134.10	9.12	9.12	9.12	9.12	9.12
VH10	VH11	83.04	143.10	83.04	83.04	83.04	83.04	83.04
VH11	VH12	52.17	143.50	52.17	52.17	52.17	52.17	52.17
VH12	VH13	34.65	202.70	34.65	34.65	34.65	34.65	34.65
VH13	VH14	20.70	142.90	20.70	20.70	20.70	20.70	20.70
VH14	VH15	28.38	86.50	28.38	28.38	28.38	28.38	28.38
VH15	VH16	91.73	149.30	91.73	91.73	91.73	91.73	91.73

VH16	VH17	25.36	129.40	25.36	25.36	25.36	25.36	25.36
VH17	VH18	36.19	128.00	36.19	36.19	36.19	36.19	36.19
VH18	VH19	49.31	140.40	49.31	49.31	49.31	49.31	49.31
VH19	VH19a	49.15	129.80	49.15	49.15	49.15	49.15	49.15
VH19	VH20	53.97	162.50	53.97	53.97	53.97	53.97	53.97
VH20	VH21	27.66	108.60	27.66	27.66	27.66	27.66	27.66
VH21	VH22	50.62	117.00	50.62	50.62	50.62	50.62	50.62
VH22	VH23	4.86	127.10	4.86	4.86	4.86	4.86	4.86
VH23	VH24	17.16	152.10	17.16	17.16	17.16	17.16	17.16
VH18	VHb1	57.09	122.00	57.09	57.09	57.09	57.09	57.09
VHb1	VHb2	13.45	332.00	13.45	13.45	13.45	13.45	13.45
VHb2	VHb3	12.80	108.00	12.80	12.80	12.80	12.80	12.80
VHb3	VHb4	18.04	133.00	18.04	18.04	18.04	18.04	18.04
VHb4	VHb5	24.28	344.00	24.28	24.28	24.28	24.28	24.28
VHb5	VHb6	19.69	41.00	19.69	19.69	19.69	19.69	19.69
VHb6	VHb7	8.53	347.00	8.53	8.53	8.53	8.53	8.53
VHb7	VHb8	22.97	329.00	22.97	22.97	22.97	22.97	22.97
VHb8	VHb9	21.00	297.00	21.00	21.00	21.00	21.00	21.00
VHb9	VHb10	29.53	316.00	29.53	29.53	29.53	29.53	29.53
VHb10	VHb11	21.33	322.00	21.33	21.33	21.33	21.33	21.33
VHb11	VHb12	23.95	306.00	23.95	23.95	23.95	23.95	23.95
VHb12	VHb13	9.19	294.00	9.19	9.19	9.19	9.19	9.19
VHb13	VHb14	18.04	336.00	18.04	18.04	18.04	18.04	18.04
VHb14	VHb15	9.51	0.00	9.51	9.51	9.51	9.51	9.51
VHb15	VHb16	10.17	241.00	10.17	10.17	10.17	10.17	10.17
VHb16	VHb17	11.48	305.00	11.48	11.48	11.48	11.48	11.48

B Segment Volumes

FROM	TO	Section Volume in m³
Ja5	Za1	60765.0
Za1	Za2	2635.58
Za2	Za3	6104.17
Za3	Za4	5339.78
Za4	Za5	5036.81
Za5	Za6	1235.8
Za6	Za7	3220.3
Za7	Za8	290.44
Za8	Za9	304.46
Za9	Za10	325.31
Za10	Za11	1444.28
Za11	Za12	68585.49
Za12	Za13	9269.57
Za13	Za14	4676.15
Za13	Za15	1474.25
Za15	Art	1328.79
Za15	Za16	489.63
Za16	Za17	153.87
Za16	Za16a	250.81
Za17	Za18	103.03
Za18	Za19	742.73
Za19	Za20	573.55
Za20	Za21	204.06
Za21	Za22	74.51
Za22	Za23	1088.87
Za23	Za24	2374.22
Za24	Za25	827.49
Za25	Za26	280.82
Za26	Za27	1101.63
Za27	Za28	1201.49
Za28	Za29	1054.59
Za29	Za30	837.87
Za30	Za31	1011.33
Za31	Za32	318.24
Za32	Za33	0.0
Za33	Za34	146.67
Za34	Za35	1004.65
Za6	HZ1	841.53
HZ1	HZ2	8399.39
HZ2	HZ3	12163.93
HZ3	HZ4	2808.61
HZ4	HZ5	2358.66

HZ5	HZ6	6.87
HZ6	HZ7	90.03
HZ7	HZ8	134.99
HZ8	HZ9	367.55
HZ9	HZ10	1470.09
HZ10	HZ11	1690.57
HZ11	HZ12	1766.56
HZ12	HZ13	293.14
HZ13	HZ14	1902.36
Za6	HZ1	841.53
HZ1	HZ2	8399.39
HZ2	HZ3	12163.93
HZ3	HZ4	2808.61
HZ4	HZ5	22382.21
HZ5	VH1	18523.05
VH1	VH2	31194.0
VH2	VHs1	33618.29
VHs1	VHs2	3273.63
VHs2	VHs3	2389.44
VHs3	VHs4	3059.31
VHs4	VHs5	374.7
VHs5	VHs6	7181.29
VH2	VH3	65861.33
VH3	VH4	37529.0
VH4	VH5	8446.05
VH5	VH6	2952.66
VH6	VH7	708.14
HZ5	HZ6	20.61
HZ6	HZ7	120.79
HZ7	HZ8	134.99
HZ8	HZ9	367.55
HZ9	HZ10	1470.09
HZ10	HZ11	1690.57
HZ11	HZ12	1766.56
HZ12	HZ13	293.14
HZ13	HZ14	11537.68
VH4	VH8	26860.04
VH8	VH9	7320.95
VH9	VH9a	5571.11
VH9	VH10	622.77
VH10	VH11	12248.84
VH11	VH12	7744.75
VH12	VH13	4679.83
VH13	VH14	2158.56
VH14	VH15	10845.01
VH15	VH16	112500.68

VH16	VH17	22337.39
VH17	VH18	13256.2
VH18	VH19	19699.1
VH19	VH19a	10408.25
VH19	VH20	7489.61
VH20	VH21	6723.75
VH21	VH22	3011.39
VH22	VH23	58.78
VH23	VH24	862.59
VH18	VHb1	3075.17
VHb1	VHb2	214.74
VHb2	VHb3	349.36
VHb3	VHb4	672.86
VHb4	VHb5	1145.11
VHb5	VHb6	573.5
VHb6	VHb7	108.64
VHb7	VHb8	467.16
VHb8	VHb9	354.76
VHb9	VHb10	400.52
VHb10	VHb11	294.07
VHb11	VHb12	401.71
VHb12	VHb13	140.82
VHb13	VHb14	216.13
VHb14	VHb15	130.76
VHb15	VHb16	151.23